Dynamic arm swinging in human walking

Steven H. Collins[1,2*], Peter G. Adamczyk[1], and Arthur D. Kuo[1]

[1]Departments of Mechanical & Biomedical Engineering, University of Michigan, Ann Arbor, MI 48109-2125, USA

[2]Department of Biomechanical Engineering, Delft University of Technology, NL-2628 CD Delft, Netherlands

* Author for correspondence (shc@umich.edu)

SUMMARY

Humans tend to swing their arms when they walk, a curious behavior since the arms play no obvious role in bipedal gait. It might be costly to use muscles to swing the arms, and it is unclear whether potential benefits elsewhere in the body would justify such costs. To examine these costs and benefits, we developed a passive dynamic walking model with free-swinging arms. Even with no torques driving the arms or legs, the model produced walking gaits with arm swinging similar to humans. Passive gaits with arm phasing opposite to normal were also found, but these induced a much greater reaction moment from the ground, which could require muscular effort in humans. We therefore hypothesized that the reduction of this moment may explain the physiological benefit of arm swinging. Experimental measurements of humans (N = 10) showed that normal arm swinging required minimal shoulder torque, while volitionally holding the arms still required 12% more metabolic energy. Among measures of gait mechanics, vertical ground reaction moment was most affected by arm swinging and increased by 63% without it. Walking with opposite-to-normal arm phasing required minimal shoulder effort but magnified the ground reaction moment, causing metabolic rate to increase by 26%. Passive dynamics appear to make arm swinging easy, while indirect benefits from reduced vertical moments make it worthwhile overall.

Keywords: locomotion; upper extremity; biomechanics; energetics; simulation; human

S1. SUPPLEMENTARY METHODS

For energetics recordings, we measured the rate of oxygen consumption (in ml O_2 s^{-1}) and carbon dioxide production (in ml CO_2 s^{-1}) using an open-circuit respirometry system (Physio-Dyne Instrument, Quogue, NY). Each trial lasted at least seven minutes, including at least three minutes to allow subjects to reach steady state, followed by at least three minutes of data recording for average oxygen consumption and carbon dioxide production during steady state. Metabolic rates were estimated using proportionality constants derived from Brockway (1987). We also measured each subject's metabolic rate for quiet standing in a separate trial and subtracted it from the rates for walking to yield net metabolic rates. All conditions were conducted in random order. Respiratory exchange ratios were found to be less than unity for all subjects and conditions.

For recording mechanical effects, we measured ground reaction forces and kinematics as subjects walked over ground-embedded force plates. Force data were recorded at 1200 Hz with two force plates (AMTI, Watertown, MA). Force plates were calibrated using a method described by Collins *et al* (2009). Kinematic data were recorded with an 8-camera motion capture system (Motion Analysis Corporation, Santa Rosa, CA) at 120 Hz. Speed was measured with two photogates, positioned 2.5 m apart and trials were discarded if actual walking speed was not within 5% of the desired speed of 1.25 m s^{-1}. We recorded at least 10 successful trials per condition for each subject. Motion capture markers were placed bilaterally on the upper and lower extremities. Marker locations included the fifth metatarsal of the foot, the heel at the calcaneus, the medial and lateral malleolli, the medial and lateral epicondyles of the knee, the greater trochanter at the hip, the anterior superior iliac spine, the sacrum, the acromion of the shoulder, the lateral epicondyle of the elbow, the posterior aspect of the wrist (i.e. just proximal to the back of the hand), and a three-marker cluster on each thigh and shank.

We measured vertical ground reaction moments and calculated vertical angular momentum for all conditions. Vertical ground reaction moment was defined as the moment between foot and ground about a vertical axis extending through the center of pressure of a single foot, as measured by force plates (also referred to as "free vertical moment," e.g. Li *et al* 2001). Vertical angular momentum was calculated from segment kinematics and defined with respect to the body center of mass (e.g. Elftman 1939) and was dominated by segment center of mass terms for the upper extremities. Anthropometric data were estimated from the data of Winter (1990). Velocities and force plate data were low-pass filtered at 25 Hz as part of this analysis. Whole-body angular momentum based on segmental analysis was compared against kinetics-based angular momentum measures, obtained by integrating moments about the body center of mass due to ground reaction forces and moments. These were verified to be roughly equivalent, with an r-squared value of 0.994 across conditions. The moment and momentum quantities are also related as follows: the rate of change of vertical angular momentum about the body center of mass is equal to the sum of the vertical ground reaction moments about the centers of pressure of each foot (zero for a foot which is in the air) plus the sum of the moments of the horizontal ground reaction forces of each foot (zero for a foot which is in the air) about the body center of mass.

We also calculated joint torques and work rates and work performed on the center of mass. To obtain joint torques and work rates, standard inverse dynamics analyses were performed in three dimensions (e.g. Winter 1990; Siegler & Liu 1997). Anthropometric data were estimated from the equations of Winter (1990) and velocities and torques were low-pass filtered at 25 Hz. Joint torques were defined with respect to the primary axis of interest, typically perpendicular to the sagittal plane. For upper body inverse dynamics, the glenohumeral shoulder joint axis was defined by a straight line across the shoulders, while the humeroulnar elbow joint axis was defined as passing through the elbow joint perpendicular to the plane defined by the upper and lower arm segments. Contact forces between the arms and the trunk were unknown in Held and Bound conditions and so upper-limb joint torques and work rates were not calculated for these conditions. We also used ground reaction forces to estimate the rate of work performed on the center of mass through each leg (referred to here as "COM work rate"; Donelan *et al* 2001; Donelan *et al* 2002), defined as the vector dot product of each leg's ground reaction force with the center of mass velocity, integrated over positive intervals to obtain work and divided by stride period to obtain work rate.

S2. SUPPLEMENTARY RESULTS

We found that Bound, Held, and Anti-Normal modes of arm swinging resulted in significantly increased ground reaction moments and vertical angular momentum as compared to Normal, accompanied by significant increases in metabolic rate. Vertical excursion of the center of mass did not change significantly. Torque and work in the shoulder and elbow joints were low in both Normal and Anti-Normal conditions. Metabolic rate in the Held condition was significantly greater than in the Bound condition. These results are summarized in tables S1 & S2.

	Normal	Bound	Held	Anti-Normal	ANOVA
Ground reaction moment (N-m)	3.03 ± 1.16	4.95 ± 1.52	4.80 ± 1.95	8.79 ± 1.65	*P* = 6.8e-09
Arms angular momentum (N-m-s)	1.06 ± 0.24	0.10 ± 0.05	0.17 ± 0.07	0.86 ± 0.20	*P* = 2.5e-10
Whole body ang. mom. (N-m-s)	0.96 ± 0.20	1.73 ± 0.17	1.67 ± 0.27	2.80 ± 0.14	*P* = 7.6e-14
Vertical COM displacement (m)	0.050 ± 0.010	0.054 ± 0.006	0.052 ± 0.007	0.054 ± 0.008	*P* = 0.15
Net metabolic rate (W/kg)	3.09 ± 0.12	3.31 ± 0.22	3.45 ± 0.25	3.93 ± 0.30	*P* = 3.0e-13
COM rate of positive work (W)	40.0 ± 5.8	44.4 ± 3.8	43.7 ± 3.0	44.4 ± 4.8	*P* = 0.0012
Peak shoulder torque (N-m)	2.45 ± 0.56	—	—	2.21 ± 0.52	*P* = 0.24
Peak elbow torque (N-m)	2.39 ± 0.21	—	—	2.30 ± 0.38	*P* = 0.55
Ankle rate of positive work (W)	32.6 ± 6.3	33.5 ± 7.1	33.0 ± 6.7	34.0 ± 6.8	*P* = 0.059
Ankle rate of negative work (W)	18.4 ± 6.0	23.0 ± 5.3	21.5 ± 5.5	22.3 ± 6.1	*P* = 0.028
Knee rate of positive work (W)	12.3 ± 4.4	15.0 ± 2.6	13.7 ± 2.8	15.9 ± 4.8	*P* = 0.013
Knee rate of negative work (W)	42.4 ± 12.1	40.8 ± 9.9	39.8 ± 10.3	39.5 ± 9.8	*P* = 0.29
Hip rate of positive work (W)	27.2 ± 5.6	27.3 ± 6.7	26.1 ± 6.4	25.8 ± 7.0	*P* = 0.20
Hip rate of negative work (W)	15.2 ± 7.2	13.7 ± 4.7	13.6 ± 5.9	13.1 ± 9.1	*P* = 0.44
Total rate of positive work (W)	72.1 ± 11.4	75.8 ± 11.5	72.8 ± 10.1	75.7 ± 9.7	*P* = 0.05
Total rate of negative work (W)	76.0 ± 16.1	77.5 ± 9.4	74.8 ± 13.1	74.9 ± 12.1	*P* = 0.72

Table S1. Summary of experimental data (mean ± s.d.) for the four experimental conditions, along with ANOVA p-values (one-way, repeated measures). Data are shown for vertical component of angular momentum for the arms and for the entire body (both about the body COM), vertical ground reaction moment about the center of pressure, vertical COM displacement, net metabolic rate (subtracting rate for quiet standing), average rate of positive work performed on COM, average rates of positive and negative work performed by each joint, and the average rate of total positive and negative work performed by all the joints.

	Normal vs. Bound	Normal vs. Held	Normal vs. Anti-Normal	Bound vs. Held	Bound vs. Anti-Normal	Held vs. Anti-Normal
Ground reaction moment	0.00024*	0.0060*	0.000016*	0.72	0.00057*	0.0012*
Arms angular momentum	0.000030*	0.000019*	0.0000052*	0.018*	0.000025*	0.0000040*
Whole-body ang. mom.	0.00017*	0.000073*	0.00000002*	0.58	0.0000095*	0.0000021*
Metabolic rate	0.0012*	0.00039*	0.0000019*	0.0019*	0.0000021*	0.0000073*

Table S2. Summary of p-values for pair-wise multiple comparisons between experimental conditions. Multiple comparison tests were conducted based on these data if ANOVA indicated significant differences across conditions. Asterisks (*) indicate statistically significant pair-wise differences for Sidak-Holm step-down procedure.

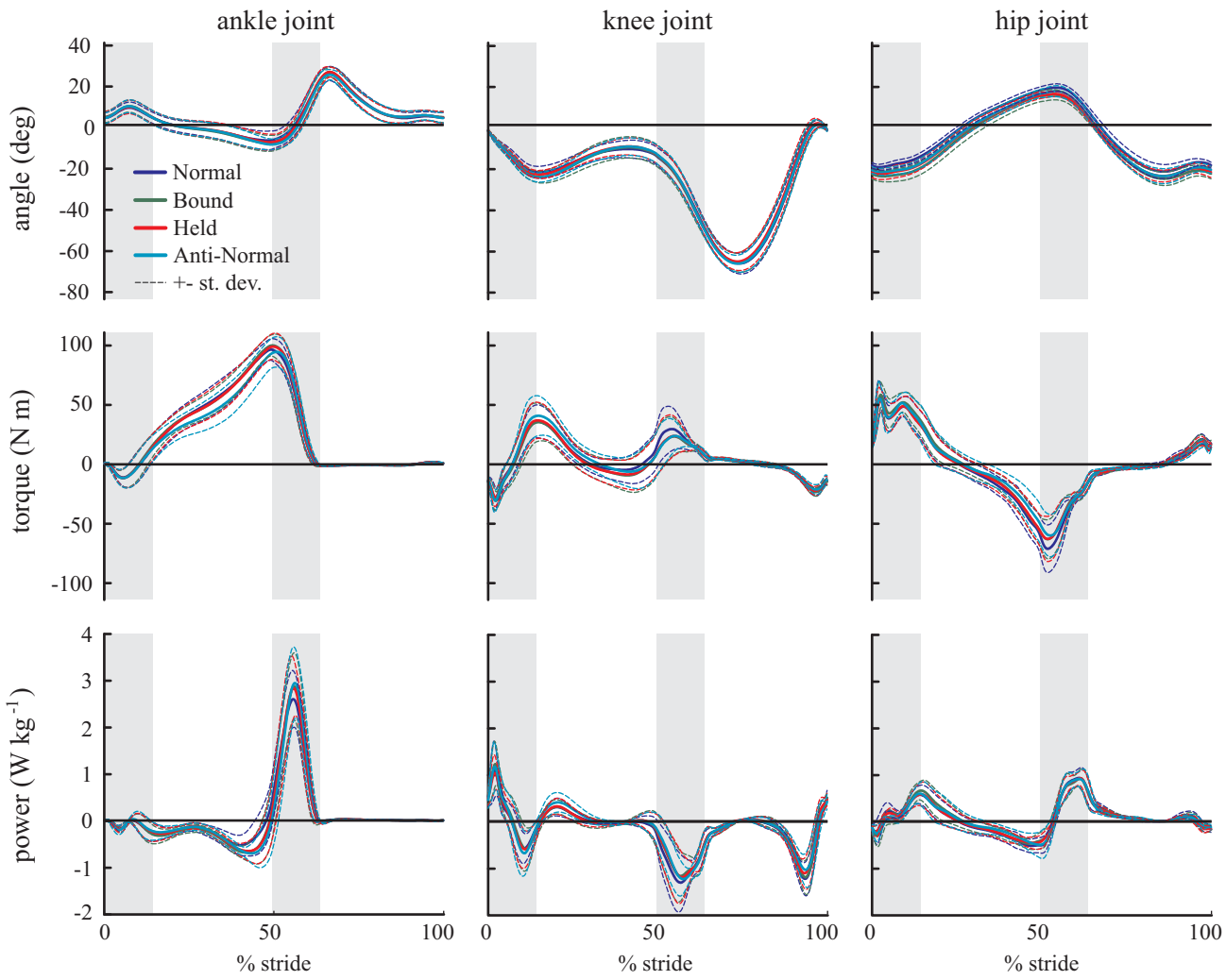

Figure S1. Lower-limb joint angles, torques, and work rates did not change substantially across conditions. Trajectories show means across all subjects, with dashed lines indicating the range of one standard deviation at each point in the stride cycle. Angles and torques are defined as positive in the extension direction.

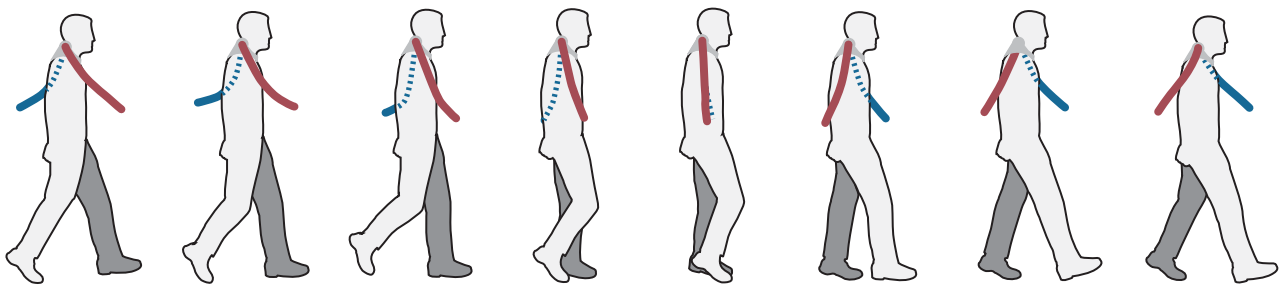

Figure S2. Passive motions of the artificial rope arms, shown swinging in the Normal mode.

S3. SUPPLEMENTARY SIMULATION DESCRIPTION

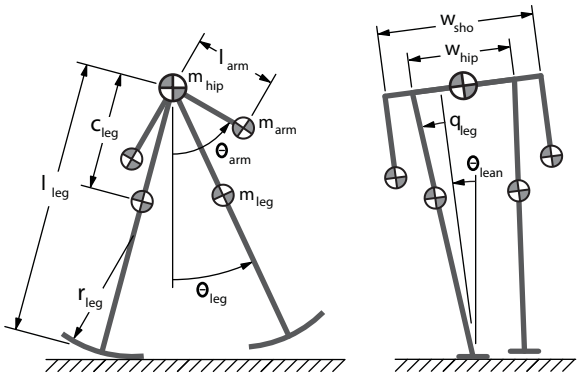

Figure S2. Schematic diagram of the passive dynamic walking model used in simulation.

(a) ***Parameter sets studied***

All of the simulations performed for the purposes of this study use the model described in the accompanying manuscript and shown in figures 1*a* & S2. In each case, a base anthropomorphic parameter set was used for most of the model parameters as follows. Throughout the simulation model, all parameters are dimensionless:

> gravitational acceleration $\boldsymbol{g} = 1$; leg length $\boldsymbol{L_{leg}} = 1$; leg center of mass position $\boldsymbol{C_{leg}} = 0.355$; leg rotational inertia $\boldsymbol{I_{leg}} = 0.016$; leg splay angle $\boldsymbol{q} = -0.075$ (feet 0.15 apart); foot radius $\boldsymbol{R} = 0.3$; hip width $\boldsymbol{W_h} = 0.3$; hip mass $\boldsymbol{m_{hip}} = 0.6$; arm length $\boldsymbol{L_{arm}} = 0.33$; shoulder width $\boldsymbol{W_{sho}} = 0.4$ (shoulders 0.2 from body center);

The remaining parameters were given three sets of values for three comparisons of interest: the Most Anthropomorphic set, the Demonstration set, and the Slow set. The Most Anthropomorphic set was used for comparisons to human gait, the results of which are displayed in figure 1b and 1c of the accompanying manuscript. In this set, the slope allows for a typical human walking speed and the hip spring acting between the legs allows for a typical human cadence (Dean & Kuo 2008). The arms represent 4% of body mass, and the legs represent 16% of body mass such that the total body mass equals 1:

> walking slope $\boldsymbol{\gamma} = 0.03$; hip spring constant $\boldsymbol{k} = 0.0175$; arm mass $\boldsymbol{M_{arm}} = 0.04$; arm rotational inertia $\boldsymbol{I_{arm}} = 0.0015$; leg mass $\boldsymbol{M_{leg}} = 0.16$;

The Demonstration set was used to create more illustrative animations of the various secondary modes of oscillation that were discovered in the model. This set exhibits nearly identical Normal, Bound, and Anti-Normal behavior as the Most Anthropomorphic set, but exhibits more easily visually distinguishable Parallel and Mid-Phase modes, animations of which are included in these supplementary materials. To better illustrate those modes of oscillation, the mass and rotational inertia of the arms were slightly reduced, the mass of the legs slightly increased (to maintain a constant body weight), and the hip stiffness slightly decreased:

> walking slope $\boldsymbol{\gamma} = 0.03$; hip spring constant $\boldsymbol{k} = 0.01$; arm mass $\boldsymbol{M_{arm}} = 0.03$; arm rotational inertia $\boldsymbol{I_{arm}} = 0.0012$; leg mass $\boldsymbol{M_{leg}} = 0.17$;

The Slow set was used to demonstrate the existence of a "double-swing" oscillation mode of the arms, a phenomenon which has been previously observed in humans at relatively slow speeds (Craik *et al*., 1976). This parameter set is based on the Most Anthropomorphic set with the walking slope reduced to as to decrease gait speed:

> walking slope $\gamma = 0.01$; hip spring constant $\boldsymbol{k} = 0.0175$; arm mass $\boldsymbol{M_{arm}} = 0.04$; arm rotational inertia $\boldsymbol{I_{arm}} = 0.0015$; leg mass $\boldsymbol{M_{leg}} = 0.16$;

(b) ***Modes of oscillation observed***

Each mode was different in quantifiable ways, some of which we report here as a reference. The primary difference between modes was in shoulder joint trajectory, and so these trajectories are presented graphically below. The efficiency of each mode was always equal to the walking slope, which was a pre-set parameter. We also defined hip stiffness *a-priori* for ease of comparison. Therefore, for each walking mode there were slightly different speeds and step lengths, reported below. As in prior 3-D models of this type (e.g. Kuo 1999) all simulated modes were unstable, primarily in side-to-side motions. Maximum eigenvalues (λ) for each mode are reported below.

Table of Mode Characteristics

	Slope	Speed	Step L	Max. λ
Most Anthropomorphic				
Normal	0.03	0.293	0.621	7.08
Bound	0.03	0.258	0.693	11.3
Anti-Normal	0.03	0.295	0.624	7.11
Demonstration				
Normal	0.03	0.285	0.632	7.82
Bound	0.03	0.257	0.676	12.3
Anti-Normal	0.03	0.287	0.634	7.83
Mid-Phase	0.03	0.281	0.622	7.68
Parallel	0.03	0.278	0.650	76.7*
Slow				
Double-Swing	0.01	0.157	0.451	15.1

* The parallel mode is a period two oscillation, leaving more time between repeatable states

Figures S3-S10 show joint angle trajectories for each mode of oscillation. Arm segment angles are shown in light blue and pink, leg segment angles are shown in red and green, and the side-to-side body angle is shown in dark blue. The arm and leg segment angles are based on the generalized coordinates used for simulation, but are approximately equal to their projections onto the sagittal plane due to the consistently small values of the lean angle. All angles are presented with respect to vertical, with positive values corresponding to positive rotations about an axis extending from the right side of the hip, i.e. with positive rotations corresponding to limb movements forwards in the direction of travel. For each mode, four consecutive steps are shown, so as to allow visualization of periodicity.

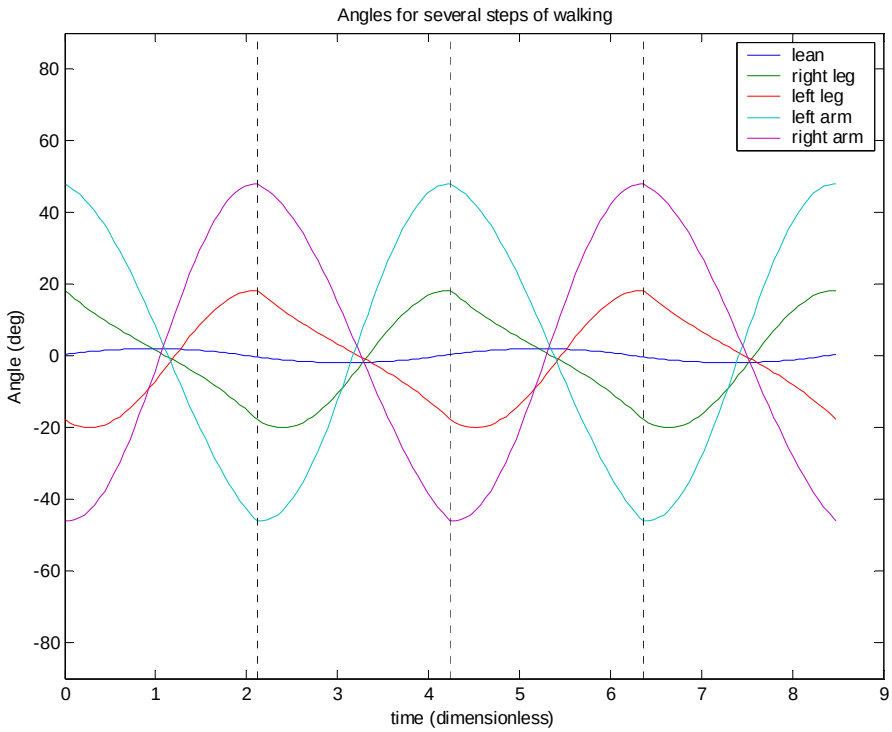

Figure S3. Joint angle trajectories for the Most Anthropomorphic parameter set Normal mode.

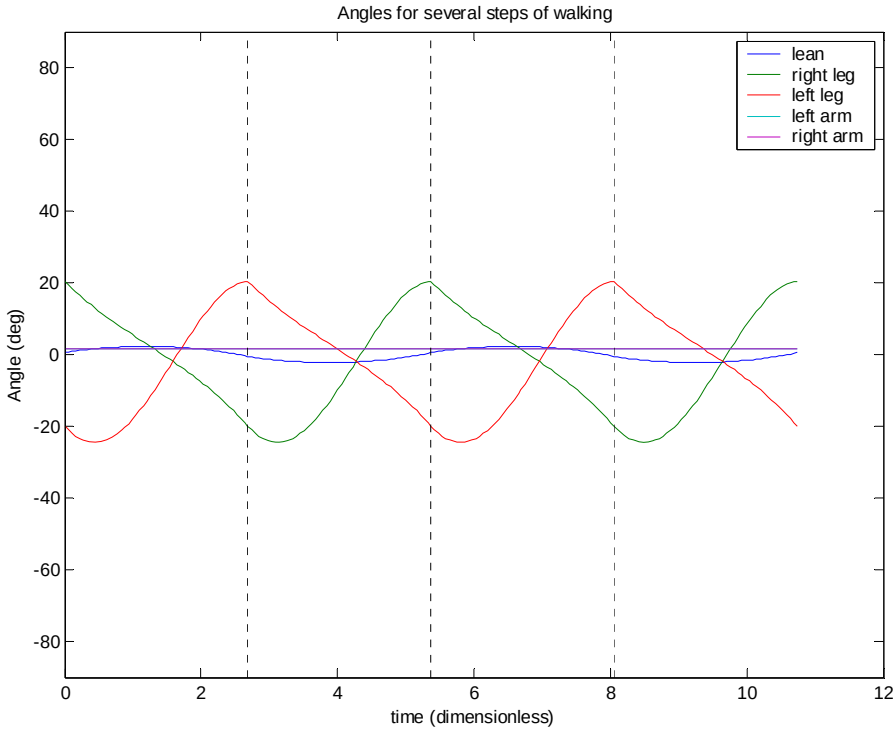

Figure S4. Joint angle trajectories for the Most Anthropomorphic parameter set Bound mode.

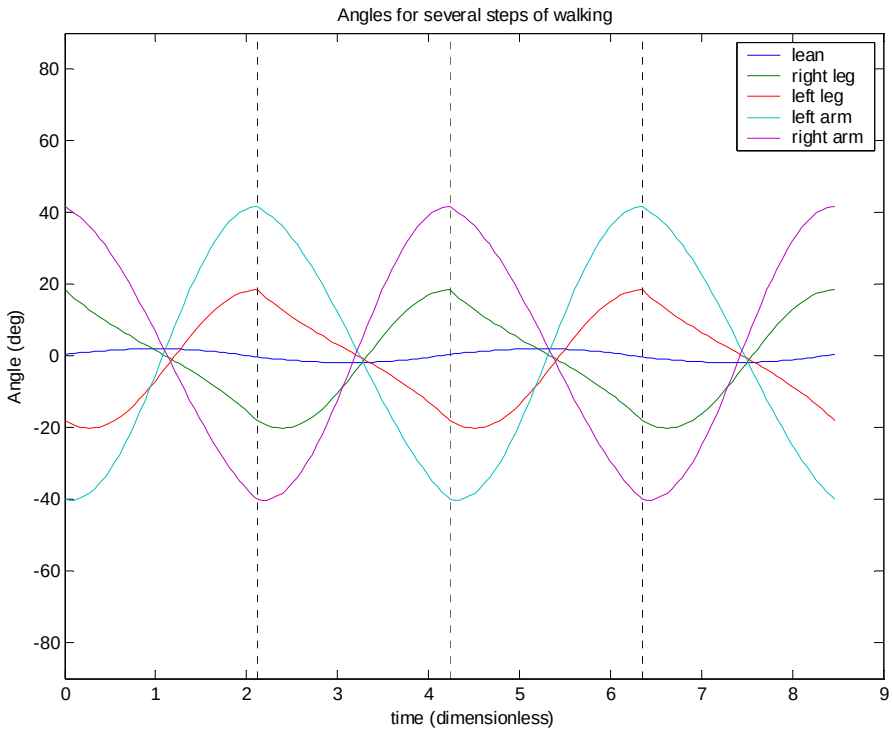

Figure S5. Joint angle trajectories for the Most Anthropomorphic parameter set Anti-Normal mode.

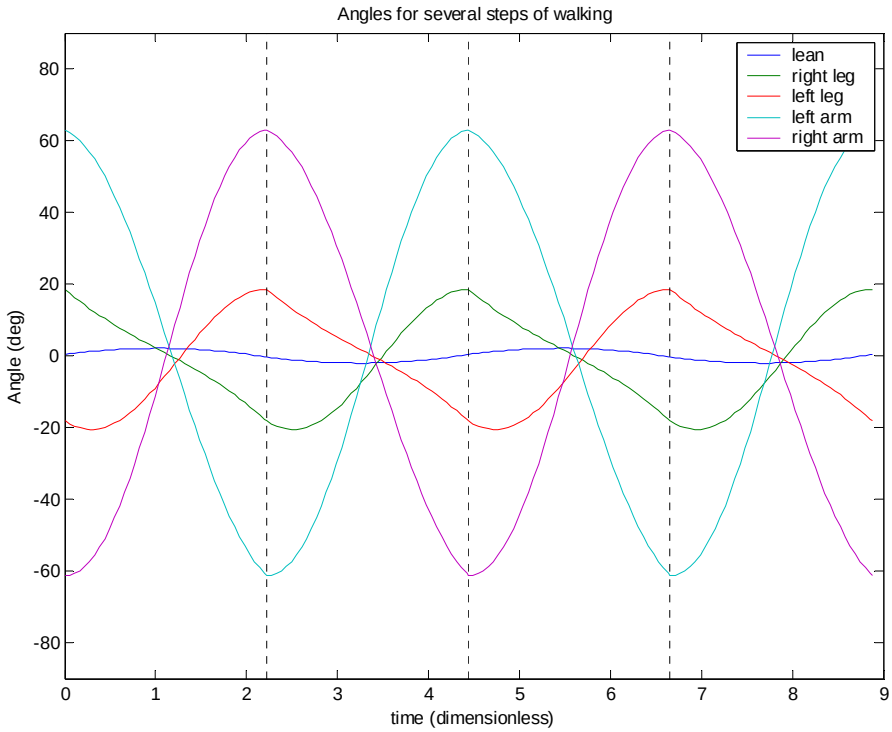

Figure S6. Joint angle trajectories for the Demonstration parameter set Normal mode of walking.

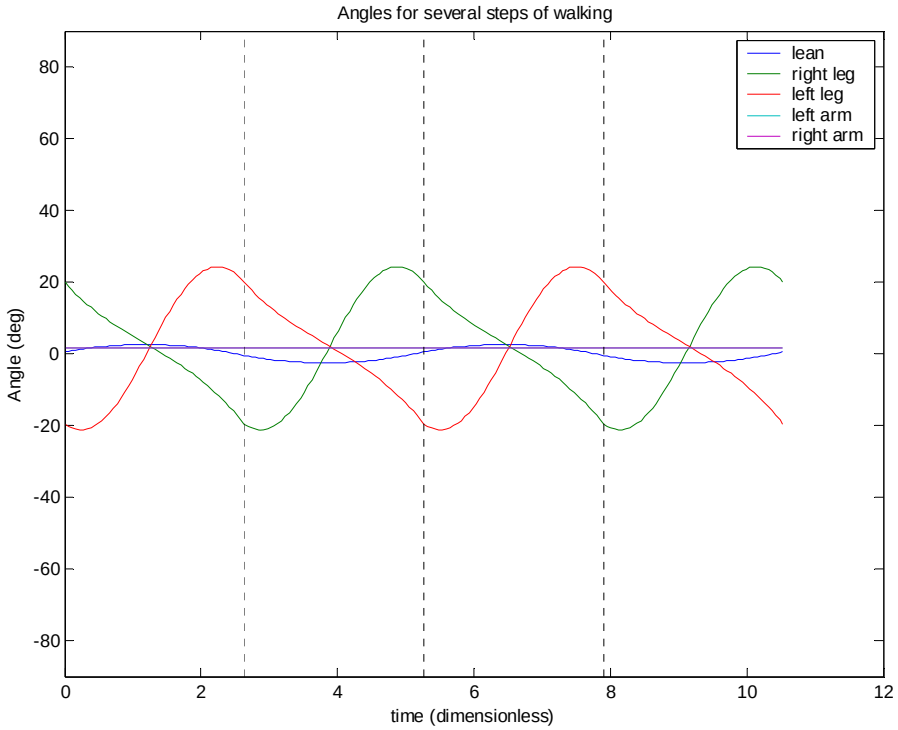

Figure S6. Joint angle trajectories for the Demonstration parameter set Bound mode of walking.

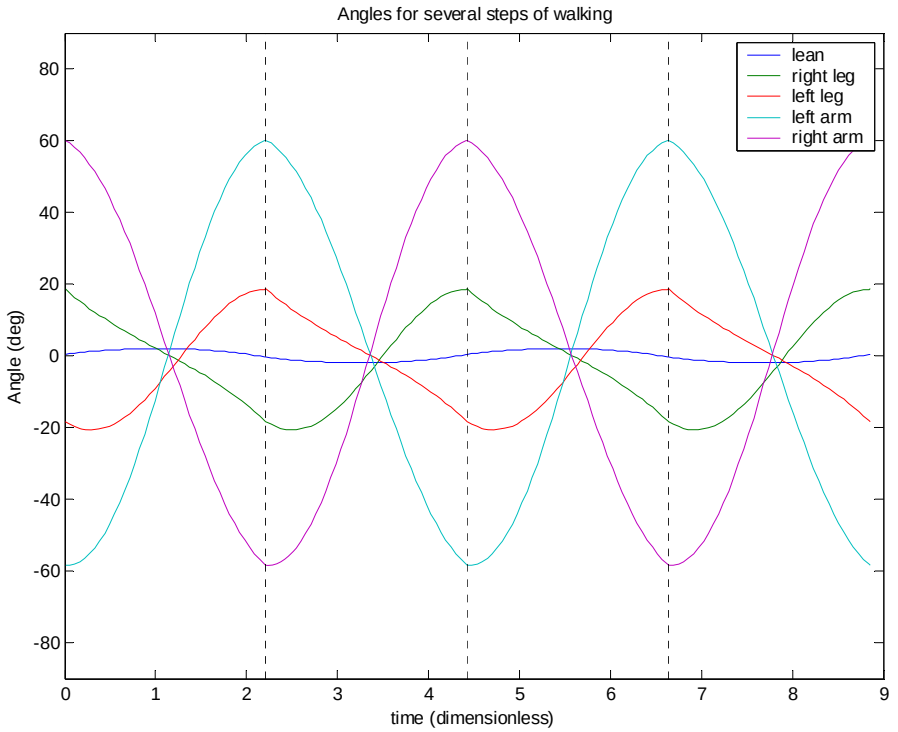

Figure S7. Joint angle trajectories for the Demonstration parameter set Anti-Normal mode.

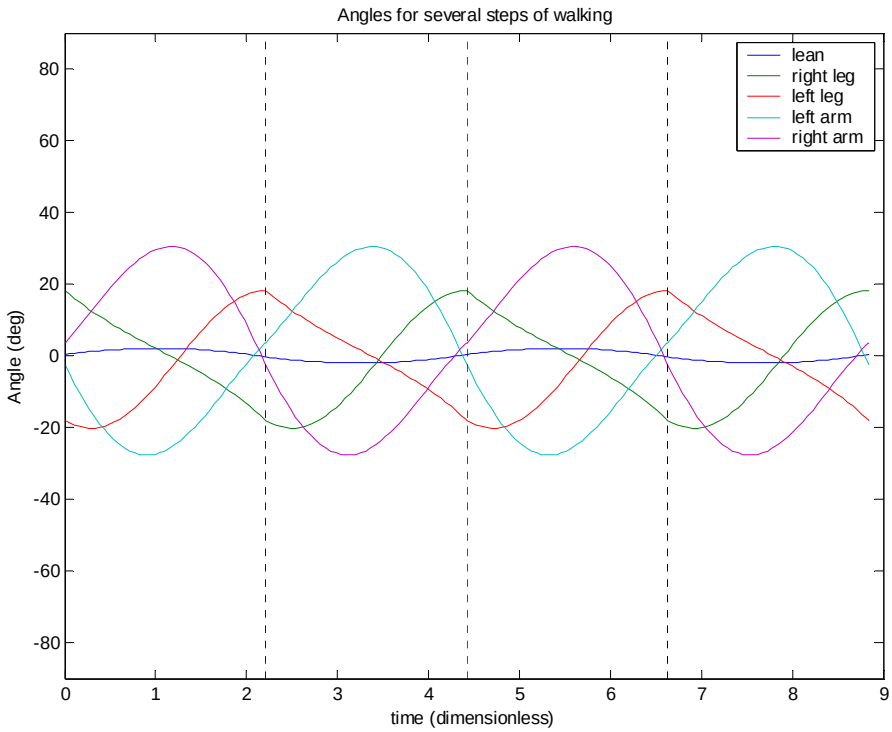

Figure S8. Joint angle trajectories for the Demonstration parameter set Mid-Phase mode of walking.

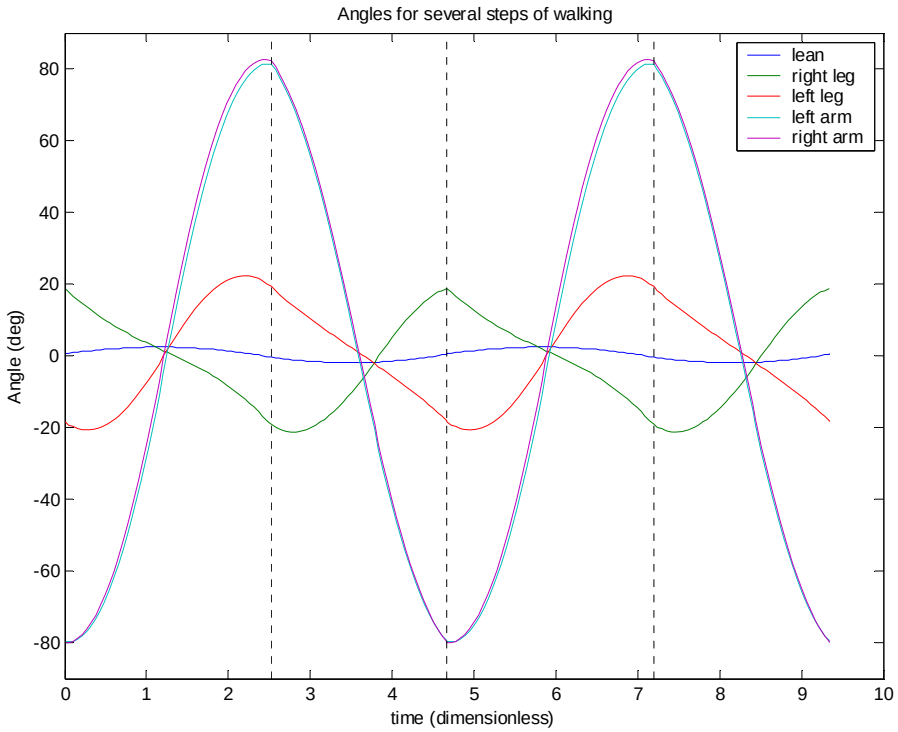

Figure S9. Joint angle trajectories for the Demonstration parameter set Parallel mode of walking.

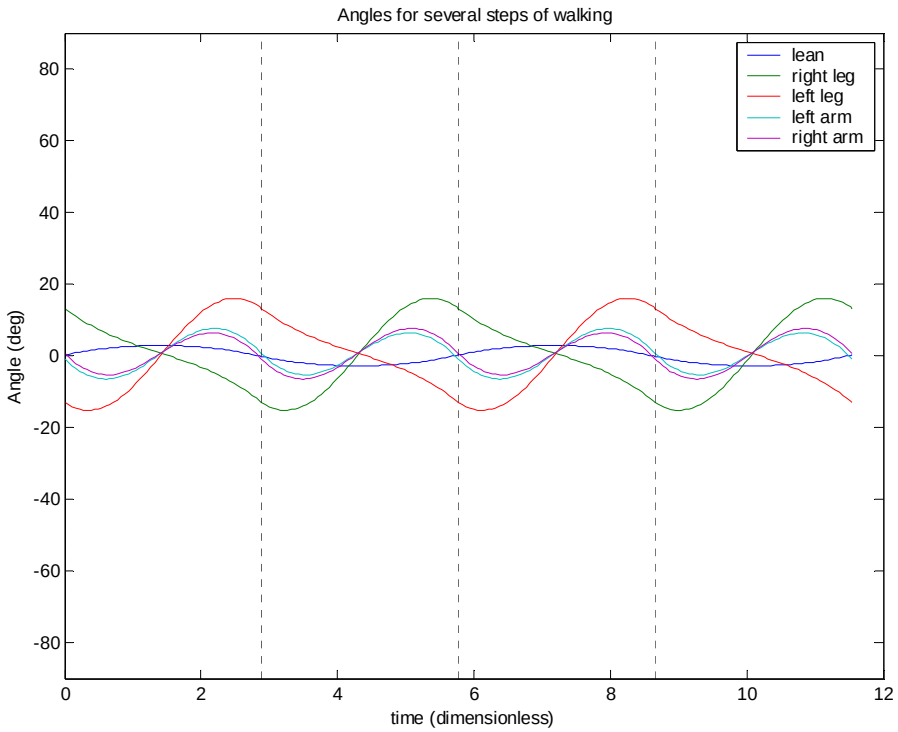

Figure S10. Joint angle trajectories for the Slow parameter set Double-Swing mode.

Animations of several of these swinging modes can be found in the accompanying supplementary videos.